Small-cone method of directly forming atomic images from energy-dependent photoelectron-diffraction data

Huasheng Wu and G. J. Lapeyre
Physics Department, Montana State University, Bozeman, Montana 59717
(Received 15 March 1994)

The method of inverting energy-dependent photoelectron-diffraction spectra collected at various emission angles to obtain images of individual atoms is applied to data for adsorbates on silicon. Since the results show considerable artifacts, an analysis of the procedure is done, which leads to a method that is model independent and relies only on the measured spectra. The result shows clean images and dimensional accuracy to about 0.2 Å. For any given point $\mathbf{R}$ in space, the method inverts spectra within a small cone whose axis is $-\hat{\mathbf{R}}$. The method is based on the experimentally determined phase and magnitude of the field generated by inversion of spectra.

The ability to experimentally determine images of individual atoms has long been a goal of science. Because the two dimensionality of surfaces and interfaces does not allow the application of the historically successful three-dimensional x-ray crystallography, surface structure determination is quite difficult. It has been a major goal in surface science to develop model-independent techniques to determine atomic structure at surfaces. Photoelectron diffraction analyzed by use of the holographic principle is emerging as a direct, model-independent method. Since the theoretical work by Barton in 1988,[1] quite a few simulations and some experimental studies have been performed. Since photoelectron diffraction is a function of both the emission angle and kinetic energy, two approaches have been used. One measures the angular dependence of core-level photoemission from the atom of interest at a fixed photon energy (kinetic energy) and then does an inversion with an angle-dependent transform to obtain an image.[1–4] To overcome limitations found in this approach, a method using multiple photon energies was used which showed some improvement.[5,6] To make full use of photoelectron diffraction phenomena, Tong, Huang, and Wei (THW) suggested another approach[7] where the energy-dependent diffraction is obtained for core-level emission from the measurement of constant-initial-energy spectra (CIS) for a set of angles which forms a grid over the full-emission hemisphere. Each CIS is inverted by a transformation over energy (wave number) and the resulting complex transform field for each CIS in the full angular set is summed to obtain an image intensity function. The power of the method was demonstrated in our previous experimental work for the Al$\sqrt{3}\times\sqrt{3}$ structure which produced an image that shows Si atoms in the first and second layers with good atomic-position values and acceptable signal to background ratio.[8] However, analysis of data from new absorbate structures on Si gives images which contain significant artifacts. To control these artifacts a modification of the analysis procedure is presented which produces high-quality images.[9] We also present data analysis that gives the phase and amplitude of the inverted CIS inversion field. The relation of this method to the small-window method of Tong, Li, and Huang[10] and the path-length-difference method of Schindler *et al.* is discussed.[11]

Applying the above full-emission hemisphere method to Si(111)$\sqrt{3}\times\sqrt{3}$-Ga data an image is obtained and shown in Fig. 1(a). The Ga sits in the T_4 site, the threefold site which has a Si atom directly below it, whose local symmetry is shown in Fig. 1(b).[12] While the image shows the site to be T_4, it contains significant artifacts that make structural determination difficult. To overcome these difficulties so as to obtain high-quality images, the data inversion procedures are examined along with the scattering formalism. By detailed analysis of the data it is found that the set of CIS most important to image formation is in a small emission region (SER) on the emission hemisphere whose center is collinear with the line between the emitting atom and one of the scattering neighbors, i.e., backscattering. Further, the CIS outside this small-emission region can be sources of artifacts. As a result, a modification to the image analysis procedure is developed which is motivated by observation of the SER phenomena. The method we introduce sums CIS transforms corresponding to a small circular set (cone) of spectra on the emission hemisphere instead of those for the full hemisphere. The procedure obtains an image intensity at each point in space by the THW inversion and summation of only those CIS's in the small cone whose axis is the line defined by the point in space and the emitter's position. This cone of fixed angular width is moved over an appropriate grid on the emission hemisphere so that the image intensity is obtained for the desired points in space. The small-cone method preserves the former method's attribute of generating a direct image by *analysis of the data only.*

To describe and characterize the emission angular behavior and its role in image formation, we examine the normalized CIS which can be described in the single scattering case, to first order by[3]

$$\chi_{\hat{\mathbf{k}}}(k)=\sum_j [\, A_{\hat{\mathbf{k}}}(k,\hat{\mathbf{r}}_j)e^{ikr_j(1-\hat{\mathbf{k}}\cdot\hat{\mathbf{r}}_j)}+\text{c.c.}\,] \tag{1a}$$

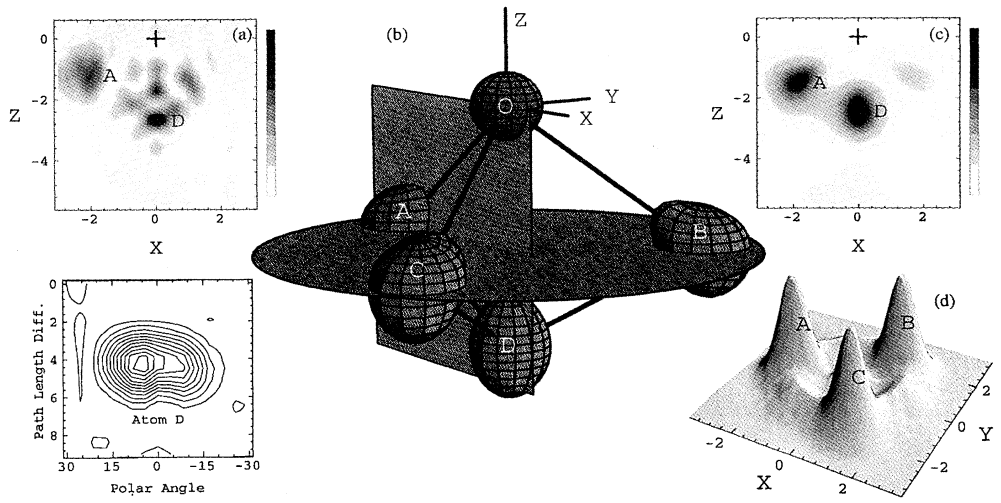

FIG. 1. Plot of image functions from the inversion of Ga $3d$ photoelectron diffraction data for the Si(111)$\sqrt{3}\times\sqrt{3}$-Ga structure; dimensions are in Å unit. (a) Cut in the x-z plane for the full-hemisphere method, where a gray scale shows the intensity with the Ga atom (origin) shown by "+." (b) Three-dimensional representation of the structure where images labeled A, B, C are the first-layer Si atoms and D the second Si, respectively. The Si images from the small-cone method are constant-intensity image surfaces at 70% of their maximum intensity. The Ga ball is added since the emitter does not "see" itself. (c) The x-z image cut. (d) The x-y image cut at $z=-1.5$ Å. (e) A contour plot of an image function at $\varphi=0°$ transformed from the data using the method in Ref. 11.

with

$$A_{\hat{\mathbf{k}}}(k,\hat{\mathbf{r}}_j)\sim F(k,\hat{\mathbf{r}}_j)F^{-1}(k,\hat{\mathbf{k}})f(k,\hat{\mathbf{r}}_j\cdot\hat{\mathbf{k}})\ . \tag{1b}$$

The emitter is at the origin, $\hat{\mathbf{k}}$ and k are the direction and amplitude of the photoelectron wave vector, and $\mathbf{r}_j$ is the jth scatterer's position vector. The factor $A_{\hat{\mathbf{k}}}(k,\hat{\mathbf{r}}_j)$ can be termed the effective-scattering factor with F and f the photoexcitation matrix element of the emitter and atomic scattering factor of the scatterer, respectively. The analysis method inverts each spectrum $\chi_{\hat{\mathbf{k}}}(k)$'s to obtain the complex CIS inversion field $\Phi_{\hat{\mathbf{k}}}(\mathbf{R})$ with the THW transform,[7]

$$\Phi_{\hat{\mathbf{k}}}(\mathbf{R})=\int_{k_{\min}}^{k_{\max}}\chi_{\hat{\mathbf{k}}}(k)e^{-ikR(1-\hat{\mathbf{k}}\cdot\hat{\mathbf{R}})}g(k)dk\ . \tag{2}$$

In the original full-hemisphere method all the CIS inversion fields are used to obtain an image intensity function from

$$U_0(\mathbf{R})=\left|\sum_{\text{all }\hat{\mathbf{k}}}\Phi_{\hat{\mathbf{k}}}(\mathbf{R})\right|^2, \tag{3}$$

where $\mathbf{R}$ is a real-space variable and $g(k)$ is a window function, for example, a Hanning function. An example of the CIS inversion field obtained from a measured CIS spectrum is shown in Fig. 2(b). To examine the properties of the CIS inversion field the general expression for the diffraction spectrum Eq. (1a) is put into the THW inversion Eq. (2). It is clear that the spatial dependence of $\Phi_{\hat{\mathbf{k}}}(\mathbf{R})$ has local maxima that form a surface, described by the condition $R(1-\hat{\mathbf{k}}\cdot\hat{\mathbf{R}})=r_j(1-\hat{\mathbf{k}}\cdot\hat{\mathbf{r}}_j)$.[7] The surface is a parabola of revolution with axis collateral to the direction $\hat{\mathbf{k}}$ used to obtain the CIS. The maximum-amplitude surface passes through the position $\mathbf{R}=\mathbf{r}_j$ of a scatterer and the maximum value for the jth atom can be written as

$$\Phi_{\hat{\mathbf{k}}}^{\max}=\int_{k_{\min}}^{k_{\max}}A_{\hat{\mathbf{k}}}(k,\hat{\mathbf{r}}_j)dk=\overline{A}_{\hat{\mathbf{k}}}(\hat{\mathbf{r}}_j)(k_{\max}-k_{\min})\ , \tag{4}$$

which is now only a function of the CIS direction $\hat{\mathbf{k}}$. The maximum of the field is proportional to the momentum-averaged effective-scattering factor, $\overline{A}_{\hat{\mathbf{k}}}(\hat{\mathbf{r}}_j)$, and its amplitude is constant on the parabolic surface when the approximations in Eq. (1a) hold. A CIS and its CIS inversion field are shown in Fig. 2. Equation (4) is now only a function of the direction used to measure the CIS and we now examine that dependence on $\hat{\mathbf{k}}$. The parabolic surface for each $\hat{\mathbf{k}}$ intersects at a given scatterer's position $\mathbf{R}=\mathbf{r}_j$. Thus the image function $U_0(\mathbf{R})$ would have a large intensity at the position of the jth atom in the ideal case when all the $\Phi_{\hat{\mathbf{k}}}^{\max}(r_j)$'s are in phase. If the latter could be true, the desired and proper image would be obtained without the need for further analysis.

In reality, the actual behavior for the amplitude and phase of $\Phi_{\hat{\mathbf{k}}}^{\max}$ with the CIS direction $\hat{\mathbf{k}}$ is not so well behaved. By using Eqs. (2) and (4), experimental values for the angular dependence of the phase and amplitude for the effective-scattering factor at the position of the jth atom, $\Phi_{\hat{\mathbf{k}}}^{\max}(r_j)$, can be obtained. Using the Si(111)$\sqrt{3}\times\sqrt{3}$-Ga data, $\Phi_{\hat{\mathbf{k}}}^{\max}(r_D)$ for the second-layer Si atom D is obtained and shown in Fig. 3. The observation shows that on the emission hemisphere there exists a small-emission region with about a 20° half width in which $\Phi_{\hat{\mathbf{k}}}^{\max}(r_D)$ has a relatively constant phase with a larger amplitude. Outside the region $\Phi_{\hat{\mathbf{k}}}^{\max}(r_D)$ has a rapidly changing phase with a smaller amplitude. The

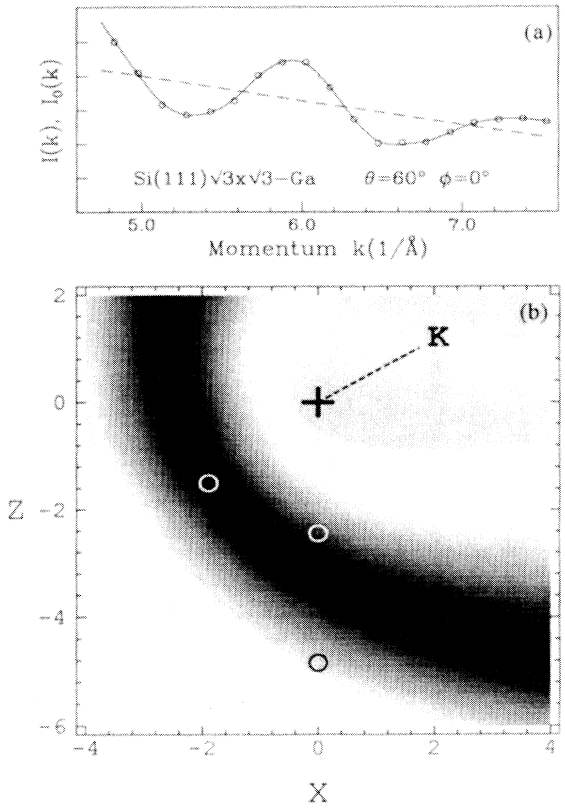

FIG. 2. (a) A representative experimental Ga $3d$ diffraction spectrum $I(k)$ (open circles) for Si(111)$\sqrt{3}\times\sqrt{3}$-Ga and the computer chosen nondiffractive curve $I_0(k)$ (dashed lines). (b) A vertical cut through the CIS inversion field plotted against the position vector in Å units where the amplitude is shown by a gray scale. The vertical plane contains the emitter (+) and the first-, second-, and third-layer Si atoms (○). The parabolic surface (cross section) formed by the maximum value of the field is evident.

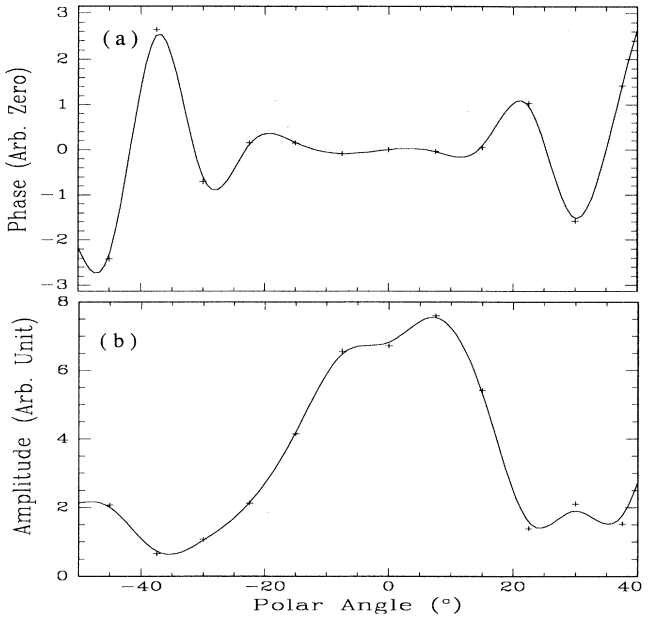

FIG. 3. The panels (a) and (b) show the angular dependence of the relative phase and amplitude of the momentum-averaged effective-scattering factor [see Eq. (4) in text] at the position of the scattering atom D for Ga $3d$ emission from Si(111)$\sqrt{3}\times\sqrt{3}$-Ga. The azimuthal angle is in a mirror plane.

center of the window is the emitter-scatterer direction, which is $\Phi=0°$ in this case.[9]

The main features of this SER behavior for $\Phi_{\hat{\mathbf{k}}}^{\max}(r_j)$ are quite general which can be demonstrated by examining the behavior of $F(k,\hat{\mathbf{r}})$ and $f(k,\hat{\mathbf{r}}_j\cdot\hat{\mathbf{k}})$ which make up $A_{\hat{\mathbf{k}}}(k,\hat{\mathbf{r}}_j)$. Here, we give a brief general explanation, and a full theoretical discussion will be presented elsewhere. For a given initial state and final state, $F(\hat{\mathbf{r}})$ is determined by the photon polarization. Since reversal of the polarization is not a physical change, a polarization reversal leaves $F(\hat{\mathbf{r}})$ essentially unchanged, which is equivalent to the behavior $F(-\hat{\mathbf{r}})\propto F(\hat{\mathbf{r}})$. Hence, the F factors in Eq. (1b) tend to cancel and $A_{\hat{\mathbf{k}}}(k,\hat{\mathbf{r}}_j)\propto f(k,\hat{\mathbf{r}}_j\cdot\hat{\mathbf{k}})$ within the small region where $\hat{\mathbf{k}}\approx-\hat{\mathbf{r}}_j$ [see Eq. 1(b)]. That is, the behavior of $\Phi_{\hat{\mathbf{k}}}(\mathbf{r}_j)$ in the SER is largely determined by just the scattering factor $f(k,\hat{\mathbf{r}}_j\cdot\hat{\mathbf{k}})$ which usually has a uniform phase and a local maximum amplitude in this SER. Outside the region there is a phase shift from the factor $F(k,\hat{\mathbf{r}}_j)F^{-1}(k,\hat{\mathbf{k}})$ which generally complicates the phase behavior of $\Phi_{\hat{\mathbf{k}}}(\mathbf{r}_j)$ [see Eqs. (1b) and (4)].

Using the properties of the effective-scattering factor, we can examine the behavior of the image function $U_0(\mathbf{R})$ for the full hemisphere method [i.e., Eq. (3)]. For those $\hat{\mathbf{k}}$ directions within the SER where the phase of $\Phi_{\hat{\mathbf{k}}}(\mathbf{r}_j)$ is quite constant, $U_0(\mathbf{R})$ builds up intensity at the jth atom position. But for those $\hat{\mathbf{k}}$'s which are outside the SER where the phase of $\Phi_{\hat{\mathbf{k}}}(\mathbf{r}_j)$ is a strong function of angle, intensity cannot build up at the jth atom position; instead, it builds up at other places which can produce artifacts. We identify two sources of artifacts that form in the full-hemisphere method and there may be others. The first source is that the parabolic surfaces from different scatterers overlap at some region of space where they have the same phase. This kind of artifact has a tendency to appear in high-symmetry directions such as rotation axes and mirror planes. The second source is from multiple scattering of the excited electron. If all $\Phi_{\hat{\mathbf{k}}}^{\max}(\mathbf{r}_j)$'s were in phase, such artifacts would be negligi-

TABLE I. Comparison of Si(111)$\sqrt{3}\times\sqrt{3}$-Ga position parameters in Å units from present work and LEED I-V analysis from Ref. 12.

a	A_x	A_z	OA	OD
This work (1)[b]	−1.9	−1.5	2.4	2.4
LEED I-V	−2.10	−1.35	2.50	2.57
This work (2)[b]	−1.9	−1.3	2.3	2.3

[a] A_x, A_z are x and z coordinates of atom A; OA and OD are the length from O (emitter) to A and D.

[b](1) and (2) correspond to with and without phase-shift correction.

ble (the details can be found in Ref. 7). Since the SER behavior of $\Phi_{\hat{\mathbf{k}}}^{\max}(\mathbf{r}_j)$'s phase limits the intensity at the jth atom position, there is the possibility for multiple scattering effects to form considerable artifacts.

To avoid artifacts and difficulties such as those discussed above, we present the following method for forming an image function:

$$U(\mathbf{R})=\left|\sum_{\hat{\mathbf{k}}\in \text{ cone }(-\hat{\mathbf{R}},w)} \Phi_{\hat{\mathbf{k}}}(\mathbf{R})\right|^2 . \tag{5}$$

For each point $\mathbf{R}$ in real space, the sum of the CIS inversion field is just over a small set of $\hat{\mathbf{k}}$ directions which are within a small cone of angular width w centered on the direction $-\hat{\mathbf{R}}$ instead of summing over all directions as described in Eq. (3).[13] The half width w, usually 15°–30°, is the only parameter and can be easily obtained from the experimental properties of the $\Phi_{\hat{\mathbf{k}}}^{\max}(\mathbf{r}_j)$ curve like those in Fig. 3.[14] The small-cone method emphasizes the most important portion of the diffraction information. As a procedure for obtaining an unknown structure, one can first use a small value of w, say 10°, to obtain a preliminary image function $U(\mathbf{R})$; then at the positions of the maximum in that function, use Eq. (2) to find the experimental curves for the phase and amplitude of the effective-scattering factor, $\Phi_{\hat{\mathbf{k}}}^{\max}(r_j)$ from which a value for w is obtained to use in the final calculation of $U(\mathbf{R})$. It is worthwhile to note that while the value of w has little effect on image positions, bigger values of w do improve the widths of the image peaks.

We add a refinement to the procedure. Scattering generally produces a phase shift which causes a small shift in nearest-neighbor distances. Because the small-cone method emphasizes backscattering, a correction to the phase shift can be made without the need to know the structure in the case of equivalent scatterers. So it is practical to do the correction which would not be the case for the full-hemisphere method.

At this point, we would like to relate our small-cone method with the small-window process used by Tong, Li, and Huang[10] to deal with the split images they obtained from processing their simulated spectra. To calculate the image function they choose spectra in a small angular window with fixed direction in the direction of the split image. The window width is obtained from the calculated atomic scattering factor f. The method is sometimes called SWEEP although the original use of the acronym was for a related phenomenon. This process, which has some utility, has been applied to our data, but it has two problems. First, the position of an atomic image depends on the choice of the direction of the small window, and there is no criterion for choosing the correct direction. Second, the window width is not determined by the atomic-scattering factor f alone, but rather by the effective-scattering factor A which is hard to calculate accurately. Our small-cone method does not have these problems since the axis of the small cone is chosen automatically as the negative $\hat{\mathbf{R}}$ direction and a width is obtainable from the experimental data.

The small-cone method is applied to experimental data for the Si(111)$\sqrt{3}\times\sqrt{3}$-Ga structure with excellent results that exemplify the power of the small-cone method.[9] The experiments were performed at the Wisconsin Synchrotron Radiation Center. A set of 76 CIS were measured for the Ga 3d core level where the angles span an irreducible symmetry element, i.e., $0°<\theta<82.5°$ and $0°<\varphi<60°$. The azimuthal angles are referenced to a mirror plane, $\varphi=0°$, and are obtained by rotation of the sample about its normal. The polar angles are selected by the rotation of the detector in the plane containing the sample normal, the photon propagation, and the photon polarization vectors. As discussed elsewhere, a smooth background function $I_0(k)$ is formed with a computer algorithm, so that the normalized CIS spectra, $\chi(k)=I(k)/I_0(k)-1$ are obtained.[8] [See Fig. 2(a) for an example.] The set of data points for $\chi(k)$ is used to form a continuous function by use of a B-spline routine. To obtain the image function with Eq. (5), a 20° half width is used as dictated by the data in Fig. 3(a). An inner potential of 10 eV and a scattering phase slope of -0.18 Å for 180° scattering[8] are also used. The resultant image, $U(\mathbf{R})$, is shown by planar cuts in panels (c) and (d) of Fig. 1. The x-z planar cut uses a gray scale for the image intensity with Ga emitter's position at the origin (the cross). The cut corresponds to that for the full-hemisphere method shown in panel (a). Shown in panel (d) is the planar cut which is through the first layer Si scatterers A, B, and C. All views show a "clean" atomic image with good signal to background ratio.[9] Finally panel (b) of Fig. 1 is actually a "three-dimensional" constant-intensity plot of the image. The positions of the Si atoms obtained from this work are compared with the low-energy electron diffraction (LEED) I-V result[12] in the first two rows of Table I. Good agreement is obtained with a discrepancy of about 0.2 Å. Values obtained without a phase-shift correction are shown in the last row of Table I.

Finally for comparison, we analyze our data with the path-length-difference transform used by Schindler *et al.*[11] since they treat the same kind of experimental data. The method has its usefulness. However, the method only transforms one spectrum at a time, which is equivalent to the zero width limit of our small-cone method. It does not make good use of the wealth of diffraction information in the experiment. Figure 1(e) shows the result by a contour plot at $\varphi=0°$, the same kind of plot as used in Ref. 11. Our angular resolution is much smaller than those in Ref. 11. It shows that the Si atom D is not in the correct direction (0°) but is off by about 7°. An even larger directional shift, about 10°, is found for our previously reported data from Si(111)$\sqrt{3}\times\sqrt{3}$-Al. Such an angular shift is reported to be a general effect and is due to large-angle scattering from nearby scatterers.[15]

In conclusion, the angular dependence of the phase and amplitude of the complex CIS inversion field was examined with experimental data which show a small emission region behavior. It is suggested that these properties are responsible for artifacts found in the image when all the spectra are processed in the full-hemisphere method. Our suggested small-cone method provides high-quality atomic images without any problems in choosing the cen-

tral direction and width for the small cone. The result from this approach for Si(111)$\sqrt{3}\times\sqrt{3}$-Ga is excellent. The numerical position values could be off by about 0.2 Å. If better numbers are desired, trial and error modeling of the spectra could be done.

We are grateful for discussions with Professor S. Y. Tong and Dr. H. Huang. We acknowledge contributions to the laboratory work by Mickey Yu. The help and support from Jim Anderson, Cliff Olson, and the Synchrotron Radiation Center staff is greatly appreciated. We are most appreciative of the support by NSF under Grant No. DMR-9107854.

[1]J. J. Barton, Phys. Rev. Lett. **61**, 1356 (1988).
[2]G. R. Harp, D. K. Saldin, and B. P. Tonner, Phys. Rev. Lett. **65**, 1012 (1990).
[3]S. Y. Tong, C. M. Wei, T. C. Zhao, H. Huang, and Hua Li, Phys. Rev. Lett. **66**, 60 (1991).
[4]S. Thevuthasan *et al.*, Phys. Rev. Lett. **70**, 595 (1993).
[5]J. J. Barton, Phys. Rev. Lett. **67**, 3106 (1991).
[6]L. J. Terminello, J. J. Barton, and D. A. Lapiano-Smith, Phys. Rev. Lett. **70**, 599 (1993).
[7]S.Y. Tong, H. Huang, and C. M. Wei, Phys. Rev. B **46**, 2452 (1992).
[8]H. Wu, G. J. Lapeyre, H. Huang, and S. Y. Tong, Phys. Rev. Lett. **71**, 251 (1993).
[9]Similar behaviors are found for Si(111)1×1-As and Si(100)2×1-As.
[10]S. Y. Tong, Hua Li, and H. Huang, Phys. Rev. B **46**, 4155 (1992).
[11]K.-M. Schindler *et al.*, Phys. Rev. Lett. **71**, 2054 (1993); V. Fritzsche and D. P. Woodruff, Phys. Rev. B **46**, 16 128 (1992).
[12]Akira Kawazu, and Hiroshi Sakama, Phys. Rev. B **37**, 2704 (1988).
[13]Independently, Hua Li and S. Y. Tong, Bull. Am. Phys. Soc. **39**, 166 (1994), have developed a small-cone method.
[14]As will be explained elsewhere, in the small-cone method the limitation of CIS spectra to small cones in **k** space is equivalent to limiting the parabolic surfaces to the same size cones in **R** space when the sets of spectra are summed.
[15]A. P. Kaduwela, M. A. Van Hove, and C. S. Fadley, Phys. Rev. Lett. **71**, 299 (1993).

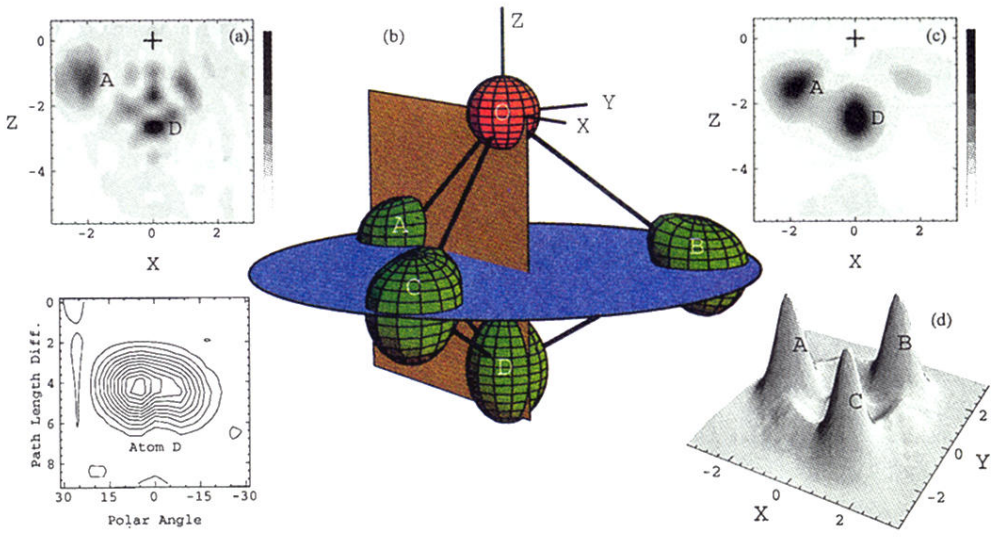

FIG. 1. Plot of image functions from the inversion of Ga 3*d* photoelectron diffraction data for the Si(111)$\sqrt{3}\times\sqrt{3}$-Ga structure; dimensions are in Å unit. (a) Cut in the *x*-*z* plane for the full-hemisphere method, where a gray scale shows the intensity with the Ga atom (origin) shown by "+." (b) Three-dimensional representation of the structure where images labeled *A*, *B*, *C* are the first-layer Si atoms and *D* the second Si, respectively. The Si images from the small-cone method are constant-intensity image surfaces at 70% of their maximum intensity. The Ga ball is added since the emitter does not "see" itself. (c) The *x*-*z* image cut. (d) The *x*-*y* image cut at $z=-1.5$ Å. (e) A contour plot of an image function at $\varphi=0°$ transformed from the data using the method in Ref. 11.

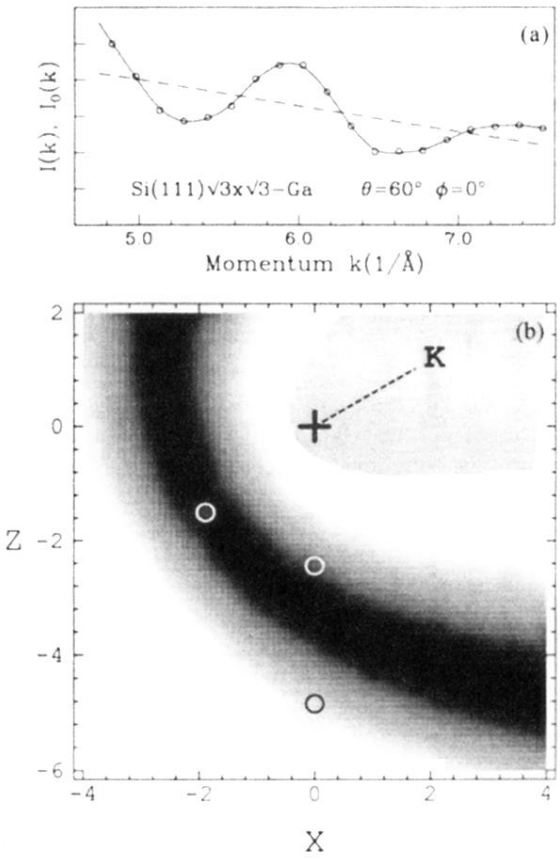

FIG. 2. (a) A representative experimental Ga 3*d* diffraction spectrum $I(k)$ (open circles) for Si(111)$\sqrt{3}\times\sqrt{3}$-Ga and the computer chosen nondiffractive curve $I_0(k)$ (dashed lines). (b) A vertical cut through the CIS inversion field plotted against the position vector in Å units where the amplitude is shown by a gray scale. The vertical plane contains the emitter (+) and the first-, second-, and third-layer Si atoms (○). The parabolic surface (cross section) formed by the maximum value of the field is evident.